IOPscience iopscience.iop.org

Home Search Collections Journals About Contact us My IOPscience

Photopolymerizable sol–gel nanocomposites for holographic recording

This content has been downloaded from IOPscience. Please scroll down to see the full text.

2009 J. Opt. A: Pure Appl. Opt. 11 024009

(http://iopscience.iop.org/1464-4258/11/2/024009)

View the table of contents for this issue, or go to the journal homepage for more

Download details:

IP Address: 147.96.14.15
This content was downloaded on 14/05/2014 at 14:41

Please note that terms and conditions apply.

J. Opt. A: Pure Appl. Opt. **11** (2009) 024009 (11pp) doi:10.1088/1464-4258/11/2/024009

REVIEW ARTICLE

Photopolymerizable sol–gel nanocomposites for holographic recording

María L Calvo[1] **and Pavel Cheben**[2]

[1] Departamento de Óptica, Facultad de Ciencias Físicas, Universidad Complutense de Madrid, E-28040 Madrid, Spain
[2] Optoelectronic Devices Group, Institute for Microstructural Sciences, National Research Council Canada, 1200 Montreal Road, Building M50, Ottawa, ON, K1A 0R6, Canada

E-mail: mlcalvo@fis.ucm.es and pavel.cheben@nrc-cnrc.gc.ca

Received 24 July 2008, accepted for publication 19 November 2008
Published 14 January 2009
Online at stacks.iop.org/JOptA/11/024009

Abstract
The research into new photosensitive materials with advanced performance for holographic applications is an active branch in material science and photonics, still challenging the field. We proposed a new class of volume hologram recording materials, sol–gel nanocomposites, with important advantages for various holographic applications, including data storage. Here we review several aspects of different types of photosensitive sol–gel glasses that we have developed. Our photopolymerizable glasses exhibit high refractive index modulation, diffraction efficiencies close to the theoretical maxima, along with low scattering and negligible shrinkage. Beside these and other practical advantages discussed in this paper, our recently developed nanocomposite glass incorporating high refractive index species has enabled fundamental studies of new optical phenomena such as the Pendellösung effect, which was observed for the first time in the optical band.

Keywords: holography, sol–gel, nanocomposite materials, holographic materials, holographic data storage

(Some figures in this article are in colour only in the electronic version)

1. Introduction

Since the early work in the first half of the 19th century by the French physicist Joseph N Nièpce who developed the first photopolymerizable substance [1], a great deal of work has been dedicated in material science to the development of new compositions with optimized photochemical properties in the optical band of the electromagnetic spectrum. In the late 1950s, the first commercial photopolymerizable composition was introduced under the name *Dycril* for printing applications [2]. Later, in 1969, Close *et al* [3] at Hughes Aircraft were the first to use a photopolymerizable system to record holograms. Since then, several research groups have developed a large number of photopolymerizable systems [4, 5], of which those of E I du Pont de Nemours and Polaroid were marketed.

Photopolymerizable materials (photopolymers) are of considerable interest for the construction of ROM (read-only memory) and WORM (write-once read-many) holographic memories, since permanent phase holograms can be formed with high refractive index modulation Δn. These materials used to have high optical quality and, unlike silver halides or dichromated gelatins, do not require complicated developing processes. Modification of the physical and chemical properties of these materials through molecular engineering is virtually unlimited, and the cost is generally low.

The physical mechanisms involving photopolymerization are well understood [5]. They typically include photon energy transfer to the sensitizer or the initiator, free radical generation and subsequent polymerization of monomer molecules to form oligomers or polymers. The reactions involved are of chain

 © 2009 IOP Publishing Ltd Printed in the UK

type and one single photon may cause the polymerization of up to $\sim 10^5$ monomer molecules. This chemical amplification of the image is the main cause of high photopolymer sensitivities compared to those for photorefractive materials. However, free radical polymerization also has a negative implication in holographic data storage applications, namely the reduction in volume (shrinkage) of the material during polymerization. This polymerization-induced shrinkage distorts the holograms, ultimately reducing the data storage capacity.

An interesting solution to the problem of shrinkage is to use a rigid matrix (binder) of porous glass impregnated with photosensitive materials (e.g. photopolymers, silver halides, dichromated gelatins, etc), resulting in hybrid organic–inorganic photomaterials [5]. In addition, porous glasses offer other advantages, such as large sample thickness, high thermal and chemical stability, improved mechanical properties, and the possibility of high quality optical polishing.

Among the class of organic–inorganic photomaterials, the sol–gel [6] materials are particularly interesting for holographic applications. The fundamental motivation for using the sol–gel reaction is to replace the high-temperature glass and ceramic fabrication techniques by a process that can take place at substantially lower temperatures, even at room temperature. In this way, organic compounds can be incorporated into inorganic matrices at a molecular level, forming organic–inorganic hybrids. This advantage opens up exciting opportunities for the development of a wide class of innovative materials, including holographic recording media.

In this article we review our work in photopolymerizable sol–gel nanocomposites. The motivation of our work encompasses two complementary aspects of material and photonic research. The first concerns development of new photosensitive nanocomposite materials by sol–gel synthesis. The second aspect concerns studies of the fundamental holographic and optical properties of these materials, including the diffusion mechanism, refractive index modulation enhancement effects, light diffraction, scattering and optical overmodulation effects. In this review paper we aim to cover these two complementary aspects of our work. This paper is organized as follows: section 2 covers material-related aspects of photosensitive sol–gel nanocomposites, including an overview of early developments (section 2.1), followed by recent developments, namely in nanocomposites with high refractive index species (section 2.2). Section 3 covers the holographic and optical effects in photosensitive sol–gel nanocomposites, including holographic grating formation (section 3.1), light scattering (section 3.2) and the optical Pendellösung effect (section 3.3). The paper ends with conclusions.

Discussions on diffusion mechanisms, refractive index modulation enhancement effects and mitigations of optical scattering are included. We also discuss the observation of an interesting phenomenon in the diffraction by volume holographic gratings recorded in these materials, namely the optical Pendellösung effect.

2. Sol–gel nanocomposite materials for holographic recording

2.1. Early sol–gel holographic nanocomposites

A number of photopolymerizable materials for holographic applications have been developed since the early 1990s [7]. However, their application for data storage was limited due to their limited thickness and shrinkage during holographic exposure [8].

The first organically modified sol–gel material capable of recording volume holograms was synthesized in 1996 [9]. This material was developed in order to overcome problems with the limited maximum thickness of commercial holographic photopolymers and shrinkage typical for acrylic-based materials. It comprised sensitizer and monomer organic species dispersed in an inorganic host matrix. In 2001, we synthesized a new sol–gel photomaterial, with a significantly improved holographic performance [10]. In this material, the organic species are dispersed in the host over domains of several nanometers. This results in a material exhibiting very low optical scattering, even if the refractive indices of the dopants largely differ from that of the host matrix. The photosensitive and photopolymerizable organic species are incorporated into the starting solution of one or more liquid glass precursors, and transformed via controlled hydrolysis and polycondensation reactions into a solid material of high optical quality. The latter is achieved along with excellent imaging properties, such as high dynamic range, sensitivity, resolution and image stability, by a combination of efficient photosensitive and photopolymerizable species with an organically modified host matrix [11]. The sol–gel reaction involved copolymerization of epoxysilanes such as (3-glycidoxypropyl)trialkoxysilane with a tetraalkoxysilane in the presence of dispersed photosensitive, photoinitiating and photopolymerizable species.

These photopolymerizable glasses were used for recording transmission volume holographic gratings in samples of various thicknesses ranging from 90 to 300 μm. Figure 1 shows the holographic recording set-up. Two collimated monochromatic s-polarized beams (1 and 2) with the wavelength $\lambda_1 = 514.5$ nm interfere at an angle 2α. This results in the formation in the material of a symmetric (unslanted) grating (with grating vector $\vec{K}$ and grating period $\Lambda = 2\pi/K$). Kogelnik's coupled wave theory to a first-order approximation provides the theoretical framework for light diffraction in such a volume grating [12]. Readout beam 3 (with $\lambda_2 = 632.8$ nm) incident on the material under the angle β is diffracted by the grating, resulting in two forward propagating beams, the zero-order beam and the first-order beams (beam 4) tuned under the angle β (scattering angle). The first-order Bragg condition (momentum matching) requires

$$\vec{k}_3 + \vec{K} = \overrightarrow{k_4} \tag{1}$$

where $\vec{k}_3$ and $\overrightarrow{k_4}$ are the wavevectors of beams 3 and 4, respectively.

Under this condition, the diffraction efficiency η is maximized and it can be expressed using Kogelnik's coupled

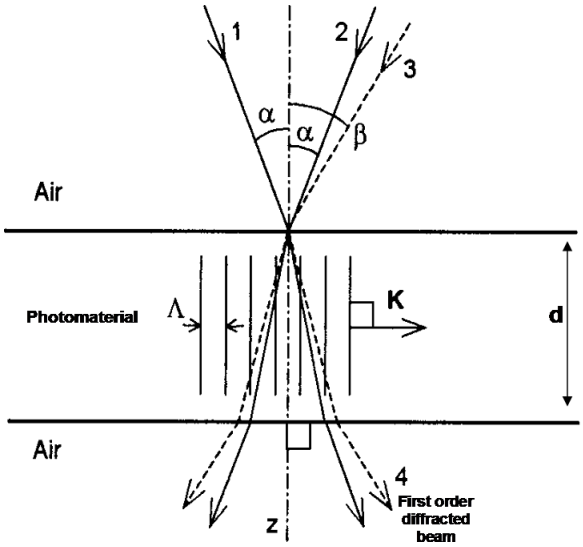

Figure 1. A holographic recording and readout set-up. Beams 1 and 2 impinge symmetrically on the holographic material with a free-space inter-beam angle 2α. The grating structure is formed within the holographic material of thickness d. The resulting grating has the period Λ and the grating vector $\vec{K}$. Readout beam 3 strikes at an angle β. Beam 4 is the diffracted first-order beam. See text for details.

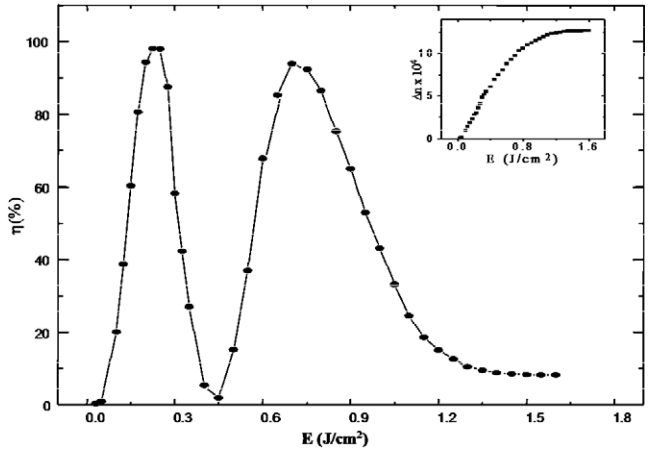

Figure 2. Diffraction efficiency as a function of exposure for a holographic grating recorded in a photopolymerizable glass [10]. Values near 100% are reached for exposures of the order of 50 J cm^{-2}, for a monolith sample of 950 μm thickness. The inset displays the evolution of the refractive index modulation as a function of the exposure.

wave theory as

$$\eta = \sin^2\left(\frac{\pi d \Delta n}{\lambda \cos\beta'}\right) \tag{2}$$

where d is the sample thickness, Δn is the grating refractive index modulation, λ is the wavelength and β' is the readout angle inside the photomaterial. It is noticed that, for small refractive index modulations, $\eta^{1/2}$ scales linearly with Δn. In a photomaterial with high dynamic range, for a progressive increase of the exposure during hologram recording, η will have an oscillatory behavior with maxima:

$$\Delta n_m = \frac{\left(m + \frac{1}{2}\right)\lambda \cos\beta'}{d} \tag{3}$$

where m is an integer number.

At the beginning of the holographic exposure there is a short induction period of virtually no growth in η. This is due to the rapid destruction of the thermal inhibitors and consumption of dissolved molecular oxygen by the photogenerated free radicals [10]. As the polymerization of the monomer starts, η increases with exposure and reaches a maximum. Figure 2 shows the typical behavior of the diffraction efficiency η as a function of the exposure energy for the photopolymerizable glass prepared according to [11]. One appreciates the high η values reaching 98% for exposure energy near 50 J cm^{-2}. The maximum refractive index modulation reported for this type of glass was $\Delta n \sim 4.5 \times 10^{-3}$ [10].

In addition to photopolymerizable systems, various photorefractive ormosils (organically modified silicates) have been developed. Photorefractive gratings with a refractive index modulation of 0.002 and a two-beam coupling gain of 444 cm^{-1} were demonstrated in an organically modified permanently poled sol–gel glass [13]. The azo-dye 2,5-dimethyl-4-(2-hydroxyethoxy)-4′-nitroazobenzene (DMHNAB) was used as a nonlinear optical chromophore. The chromophore molecules were covalently bonded to the silica glass backbone in order to achieve the high dye concentration needed for efficient nonlinear optical properties. This also avoids dye crystallization often observed in guest–host photorefractive polymers. 2,4,7-trinitro-9-fluorenone (TNF) was used as a photosensitizer and *N*-ethylcarbazole (ECZ) as the charge-transporting agent, both being present as guests in the glass, i.e. without being covalently attached to the matrix. Excellent resistance against chromophore crystallization was achieved by covalently bonding the chromophore. The high stability of the electric-field-induced chromophore alignment is due to a gradual heat-induced densification of the gel with an initially low glass transition temperature (T_g) during electric field poling, eventually yielding a high-T_g hard glassy film. This densification process is essential for slowing down diffusive randomization of the chromophore alignment and for improving the glass's mechanical, electrical and thermal properties. Similar materials, with high glass transition temperatures, are desirable, for example, in long-term data storage and electro-optical modulators.

2.2. Advanced compositions: organic–inorganic nanocomposites with high refractive index species (HRIS)

Attempts have been made to improve the refractive index modulation of a photopolymerizable medium by incorporating diffusible high refractive index species (HRIS) [14–16], for example, titania nanoparticles. Volume holographic gratings with refractive index modulations of up to 0.015 have been reported [17]. However, the incorporation of nanoparticles in general tends to increase the scattering noise, in part due to nanoparticle agglomeration. The scattering level can be substantially reduced by a modified chemical composition

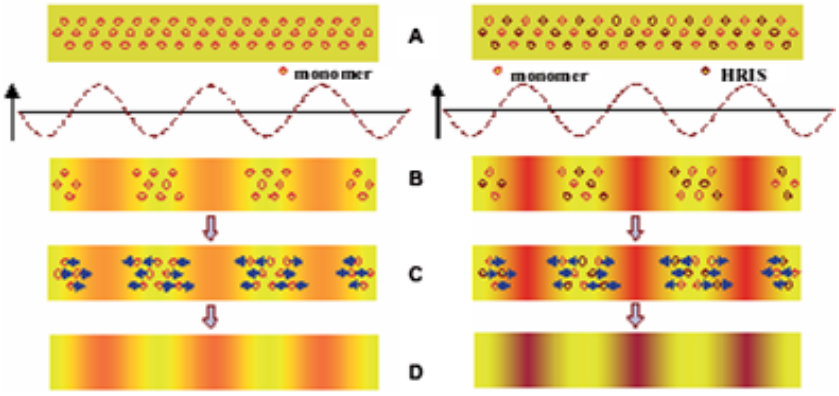

Figure 3. Formation of the refractive index grating in a photopolymerizable material based on a conventional (Colburn–Haines) monomer diffusion mechanism (left) and in a photopolymerizable material modified with HRIS (right) (after [18]).

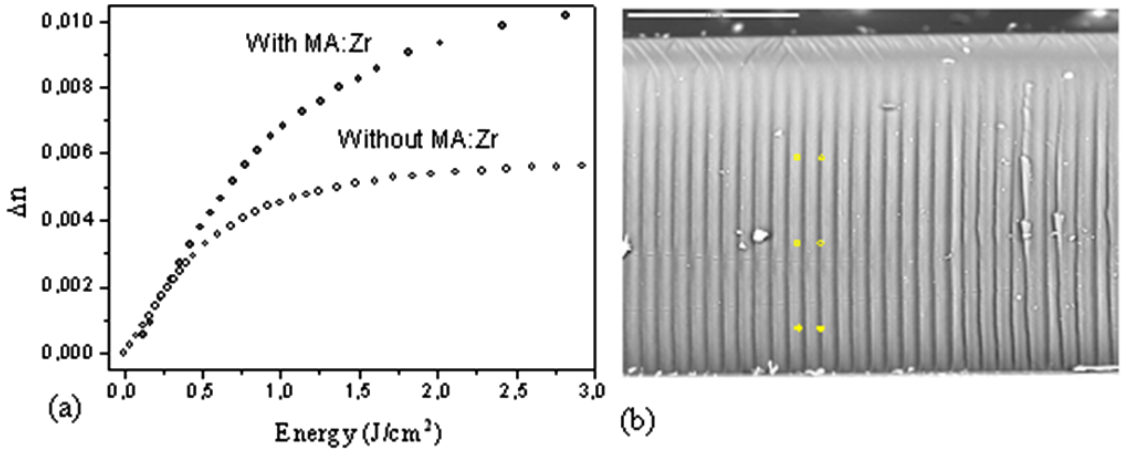

Figure 4. (a) Refractive index modulation of volume gratings recorded in samples with and without the HRIS (MA:Zr). Sample thickness is 35 μm. (b) Scanning electron microscope image of a grating recorded in a sample with the HRIS. Sample thickness is 250 μm and the grating spatial frequency is 100 lines mm^{-1} (after [18]).

of our previously described photopolymer glass. This improvement can be achieved by incorporating the HRIS at the molecular level.

We have developed a new sol–gel holographic material exhibiting a large Δn incorporating a high-refractive-index MA:Zr molecular complex, namely zirconium isopropoxide chelated with (metha)acrylic acid (MA) in a sol–gel matrix [18]. A general formulation of the process involves hydrolysis of silicon and zirconium alkoxides ($\{Si, Zr\}(OR)_n$ and R an alkyl group), followed by a polycondensation reaction:

$$\{Si, Zr\}(OR)_n + nH_2O \rightarrow \{Si, Zr\}(OH)_n + nR(OH)$$

$$\{Si, Zr\}(OH)_n \rightarrow MO_{n/2} + n/2H_2O.$$

The large Δn in our material relies on the ability of the high-index MA:Zr complex to diffuse and thus contribute to grating formation upon inhomogeneous illumination (see figure 3). This mechanism may be compared with the conventional Coburn–Haines model [19] of volume holographic grating formation in a photopolymer film (left side of figure 3). On photoinduced polymerization of the (metha)acrylic acid, diffusion driven by a concentration gradient of the MA:Zr complex takes place from the dark to the light regions of the interference pattern. By incorporating the high-index MA:Zr species in the host, the refractive index modulation of the material is increased to $\Delta n \sim 0.01$, compared to $\Delta n \sim 0.005$ in the sample without the high-index species (see figure 4(a)). Thus, in this photomaterial, the holographic grating forming mechanism involves co-directional diffusion of two types of molecules, the monomer and the HRIS, increasing the refractive index contrast between the dark and bright regions of the interference pattern (see the right-hand side of figure 3).

An important property of this material is that, compared to the photopolymers with dispersed high-index (TiO_2) nanoparticles, scattering is markedly reduced as a consequence of the molecular nature of MA:Zr. Optical scattering in sol–gel nanocomposites will be discussed in detail in section 3.3.

Finally, in table 1 comparative data are presented for diffraction efficiency and refractive index modulation for

Table 1. Selected physical properties of volume holographic gratings recorded in photopolymerizable glasses.

Composition	Δn	Diffraction efficiency (η%)	Reference
Silica gel MMA ORMOCER[a]		93 (54 line pairs/mm @ 632.8 nm)	[9] (1996)
Photopolymer-filled nanoporous *Vycor* glass	1×10^{-5}	2.3 (1400 line pairs/mm @ 632.8 nm)	[7] (1999)
Photopolymerizable glass with inorganic glassy host	3×10^{-4}	98 (100 line pairs/mm @ 632.8 nm)	[10] (2001)
AA and BAA sol–gel processed films[b]	1×10^{-3}	93 (676 line pairs/mm @ 632.8 nm)	[8] (2004)
Photopolymerizable glasses with Zr-based HRIS[c]	1×10^{-2}	99 (500 line pairs/mm @ 632.8 nm)	[18] (2006)
Highly transparent ZrO_2 nanoparticle-dispersed acrylate photopolymers	3×10^{-3}	(1000 line pairs/mm @ 632.8)	[20] (2006)

[a] Silica gel MMA ORMOCER: silica gel methyl methacrylate organically modified ceramic.
[b] Acrylamide AA, N, N'-methylenebis acrylamide BAA.
[c] High refractive index species based upon MA:Zr (MA: methacrylic acid).

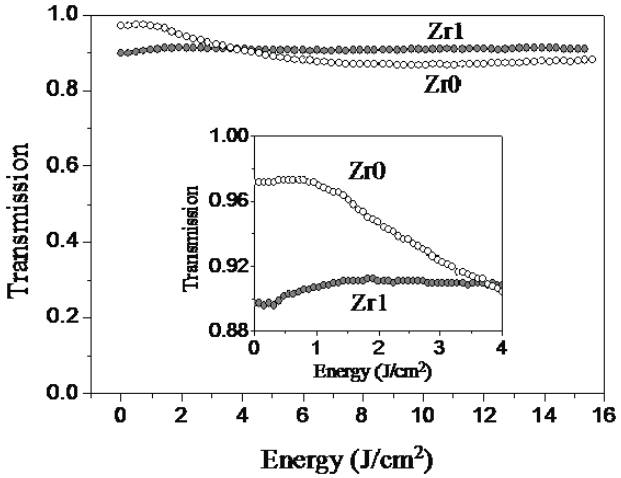

Figure 5. Transmission as a function of the exposure energy for Zr0 (photopolymerizable glass without MA:Zr complex) and Zr1 (with MA:Zr complex) samples measured during the noise grating recording experiment. Inset: detail of the transmission for an exposure range of 1–4 J cm^{-2}. The samples were exposed to a coherent *s*-polarized single beam of wavelength 532 nm and intensity 5 mW cm^{-2}.

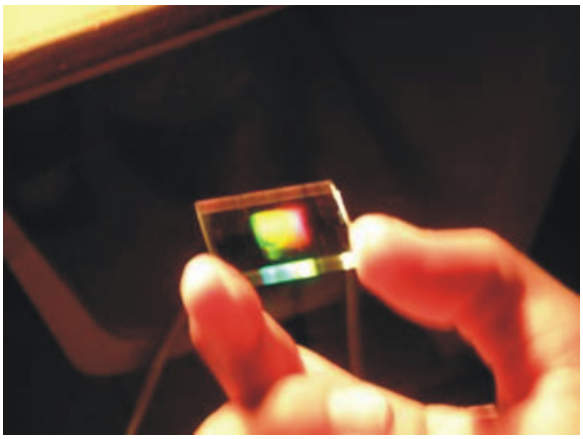

Figure 6. Dispersion of a holographic grating in the nanocomposite glass with MA:Zr HRIS under white light illumination. The grating spatial frequency is 500 line pairs mm^{-1} (after [17]).

various organic–inorganic photomaterials, in chronological order. For comparison, we have also included data corresponding to some nanoparticle-dispersed photopolymers.

3. Holographic performance and optical effects in sol–gel photosensitive nanocomposites

3.1. Holographic grating formation mechanism

The study of volume holographic grating formation dynamics, particularly the temporal evolution of the refractive index modulation, is essential for understanding the properties of the holographic recording media. The diffraction efficiency temporal evolution has been studied for various types of holographic photomaterials. For example, it has been used to analyze the role of thermally activated processes in the decay of the diffraction efficiency in photorefractive crystal gratings ($LiNbO_3$:Fe) [22]. Several analyses of monomer diffusion time have been performed in polyvinyl/acrylamide materials [23]. Similar studies have been carried out for diffraction gratings and diffusion coefficient determination of acrylamide in sol–gel glasses [24, 25]. It was shown how the spatial modulation of the refractive index and its evolution over time is influenced by nonuniform polymerization and the diffusion of monomers. A diffraction efficiency of 55% was reported for this material for an energy exposure of 8 mJ cm^{-2}. Recently, Gallego–Gomez *et al* have monitored the temporal evolution of the diffraction efficiency for various geometries of holographic gratings recorded in organic photomaterials [26]. Other interesting phenomena, such as non-local grating recording in a non-photorefractive material, have recently been reported [13, 26].

We have carried out various experiments to monitor holographic grating evolution in photopolymerizable glasses incorporating HRIS. The evaluation of the recorded holographic gratings was conducted by real time monitoring diffraction efficiency under Bragg condition, studying the temporal evolution of the kinetics of grating formation [27]. Figure 7 shows the temporal evolutions of the diffraction efficiency (left column) and the resulting angular selectivity (right column) for three analyzed samples. The holographic recording parameters

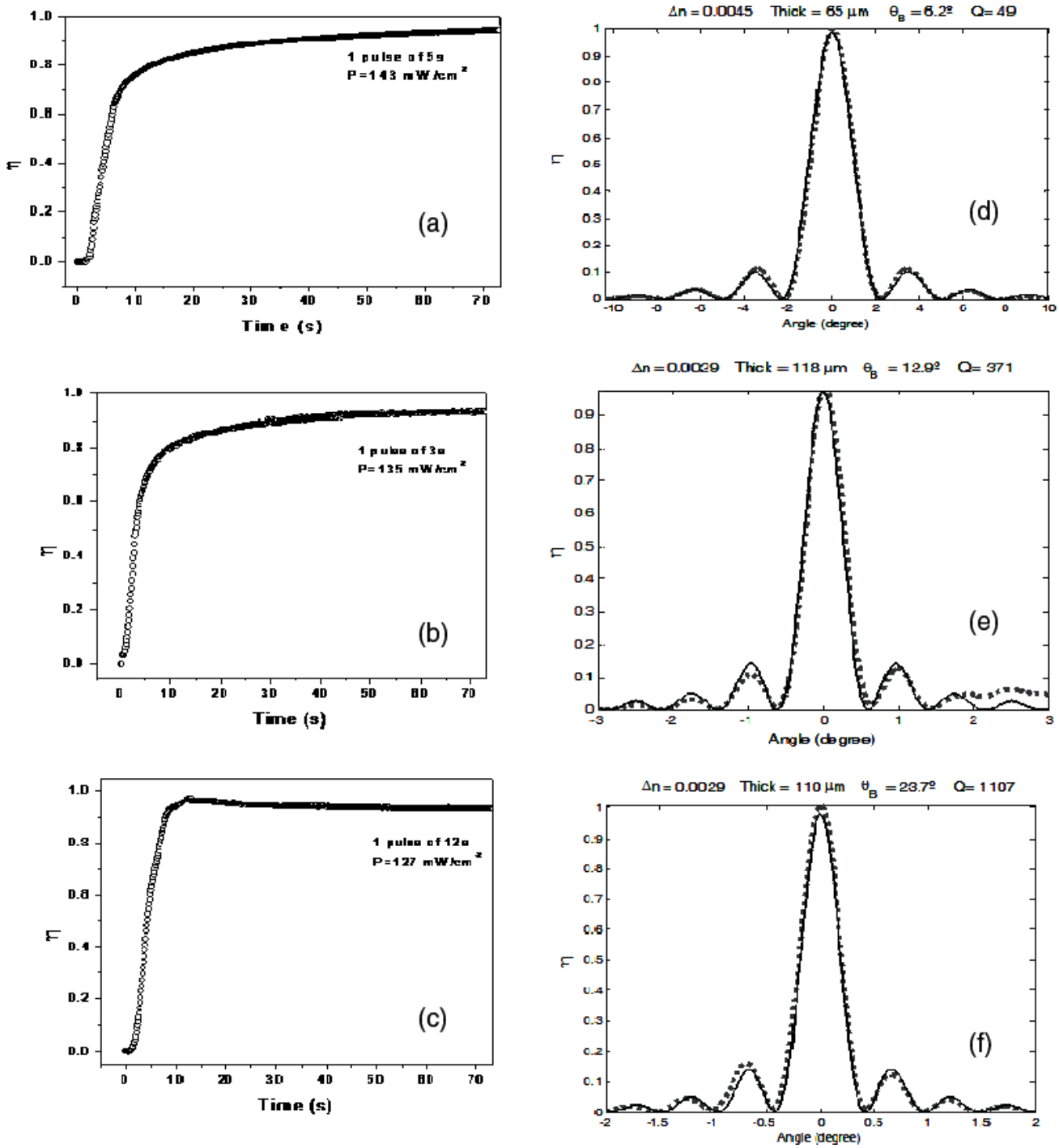

Figure 7. Diffraction efficiency temporal evolution measurements with a non-actinic He–Ne laser probe beam for three holographic gratings recorded in the nanocomposite material with HRIS. The gratings' spatial frequencies are: 556, 1135 and 2031 lines mm^{-1}. Left column ((a), (b), (c)): temporal evolution of grating diffraction efficiency at Bragg condition during (gray region) and after holographic exposure. Right column ((d), (e), (f)): measured angular selectivity of the corresponding grating (dots) and the fits according to first-order approximation Kogelnik's coupled wave theory (solid lines). Parameters: grating thickness, recording time, writing beam irradiance, Klein–Cook parameter (Q), readout beam Bragg angle (θ_B) and refractive index modulation Δn (after [27]).

are indicated in the figure, including the pulse duration, writing beam irradiance (P), thicknesses, the grating spatial frequencies, refractive index modulation Δn, Bragg angle (θ_B) and Klein–Cook Q parameter [28]. The solid curves in the angular selectivity panels (right column) were calculated using Kogelnik's coupled wave theory to a first-order approximation.

The monomer dark diffusion transient was studied by Piazzolla *et al* [29] for a one-component free-monomer diffusion model. They demonstrated that the variation of the recorded grating modulation $\Delta n(t)$ during dark diffusion transient follows an exponential law. For our material, the model can be extended to include the contribution of

two diffusible components, namely the acrylic monomer 2-phenoxyethylacrylate (POEA) and the MA:Zr complex, according to the following equation:

$$\Delta n - \Delta n_0 = c_{\mathrm{M}}\left[1 - \exp\left(-\frac{t}{\tau_{\mathrm{M}}}\right)\right] \pm c_{\mathrm{Zr}}\left[1 - \exp\left(-\frac{t}{\tau_{\mathrm{Zr}}}\right)\right] \quad (4)$$

where Δn and Δn_0 are the refractive index modulations after and before the exposure, respectively; c_{M} and c_{Zr} are the contributions of the first harmonic term of the free-monomer concentration and of the MA:Zr complex, respectively; and τ_{M} and τ_{Zr} are the diffusion times of the monomer and the MA:Zr complex, respectively. The positive and negative signs in equation (4) account for two possible diffusion mechanisms, namely equal signs for both components corresponding to in-phase grating formation, and opposite signs indicating two gratings dephased by 180°. The latter effect, i.e. the counter diffusion, has been recently reported in nanoparticle-dispersed photopolymers [30]. From equation (4) one realizes that the counter diffusion produces a decrease in the refractive index modulation that is an undesirable phenomenon in holographic materials when large dynamic range is aimed for. As we have demonstrated, the counter diffusion does not take place in our material, and co-directional diffusion, hence refractive index modulation enhancement, was confirmed. This is particularly an important fact for practical implementations, including holographic and diffractive optical elements as was studied earlier by Däscher *et al* [31].

3.2. Light scattering

The evolution of scattering noise can be monitored, for example, by optical transmittance measurements during holographic recording (figure 5). Scattering originates by the inhomogeneities in the volume and the surface of the photomaterial. Scattered light induces noise gratings in the hologram formation, hence reducing dynamic range and deteriorating crosstalk, for example in the case of hologram multiplexing. It is expected that, in the photopolymerizable glasses incorporating HRIS at a molecular level, scattering effects should be reduced. To evaluate the magnitude of the scattering effects in our material, we first used the technique as in Sanchez *et al* [16], where the intensity of a probe He–Ne laser (*s*-polarized, $\lambda = 632.8$ nm) beam was compared with the sum of intensities of the zero order, the -1 and the $+1$ orders and the Fresnel reflection. Samples with and without MA:Zr molecular complex of various thicknesses were studied. This technique gives a conservative estimate of the scattering coefficient α because the absorbed light is accounted for as the scattered light. The scattering coefficients α found for materials without HRIS (sample Zr0) and with HRIS (sample Zr1) are 2×10^{-3} $\mu\mathrm{m}^{-1}$ and 1.2×10^{-3} $\mu\mathrm{m}^{-1}$, respectively. Note that for a material of 15 μm thickness, these values would correspond to ∼3% (Zr0) and ∼1.8% (Zr1) of scattered light.

No scattering increase upon incorporating HRIS (i.e. comparing the sample Zr1 with HRIS and the sample Zr0 without HRIS) suggests the comparatively small size domains of HRIS in our nanocomposite material. Furthermore, in our material with HRIS incorporated at the molecular level, compared to previously reported holographic materials (nanoparticle HRIS [16]), the scattering is significantly (∼8×) reduced. This is a remarkable improvement, which we attribute to the molecular nature of HRIS in our nanocomposite glass.

In the second experiment, we used a technique by Frantz *et al* [21] and previously used for characterization on the Aprilis ULSH photopolymer. Two samples, Zr0 and Zr1, were used with equal thickness of 92 μm. A single recording beam (*s*-polarized, $\lambda = 532$ nm) of intensity 80 mW cm^{-2} was illuminating the sample and the photoinduced transmittance changes arising from formation of noise gratings were monitored in real time. While there is approximately a 9% decrease in transmittance for sample Zr0, this can be attributed to the observed surface roughness. There is virtually no transmittance degradation in the Zr1 sample, indicating that the scattering is very weak even upon incorporation of HRIM. The very weak character of the noise grating was also confirmed by the noise grating angular selectivity measurement (see [18] for details).

A simple visual observation often provides a valuable insight into grating optical quality, including spatial homogeneity, scattering and diffraction efficiency. Figure 6 shows an image of the observed dispersion as the holographic grating is illuminated with white light. High diffraction efficiency is observed for the whole visible range [17].

3.3. Optical Pendellösung effect

3.3.1. Fundamentals and theoretical framework. The recent availability of highly efficient new photopolymerizable glasses incorporating HRIS has allowed the experimental observation of anomalous diffraction effects not previously reported in the optical band. This is the case of the so-called Pendellösung fringes. The dynamical theory of x-ray diffraction first formulated by Ewald predicts the Pendellösung effect [32]. This is the approach we are following here. The theory and experimental verifications were discussed in detail by Batterman and Cole [33]. The coherent splitting of the incident beam will result in a radiation periodic beating at different depths of the grating. The experimental observation of this effect was not trivial since it requires thick almost perfect crystal structures, or amorphous highly modulated optical media, with large diffraction efficiency and dynamic range. Pendellösung fringes were first observed in 1968 by Shull for the interference formed by the diffraction of slow neutron beams by thick crystals of SiO_2 with thicknesses ranging from ∼0.3 to 1 cm [34]. The overmodulation was caused by the coherent splitting of the incident wave when diffracted by the periodic crystalline structure. The Pendellösung fringe structure appears as a consequence of the interference between two components of the wavefunction, which result in solutions of the Schrödinger wave equation, within the framework of the dynamical theory of diffraction [32]. This phenomenon is formally analogous to the transfer of energy between two coupled pendulums, hence its name as introduced by Ewald. One application of this effect was the experimental determination of the unit cell of the crystal structure and

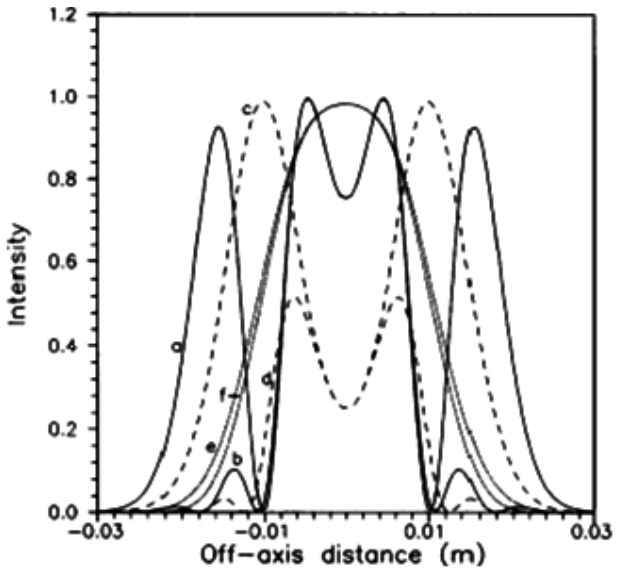

Figure 8. Calculated transverse intensity profiles for a Gaussian beam diffracted by volume holographic gratings for different values of medium thickness T and wavelength shift $\delta\lambda$ (chromatic dephasing). Numerical parameters: dielectric permittivity modulation: 0.025; dielectric permittivity of the photomaterial prior to exposure: 2.25; wavelength: $\lambda = 500$ nm; Gaussian beam radius: 0.01 m; d: distance source–hologram: 0.1 m; Curves (a) $T = 200\lambda$, $\delta\lambda = 10$ nm; (b) $T = 200\lambda$, $\delta\lambda = 50$ nm; (c) $T = 100\lambda$, $\delta\lambda = 20$ nm; (d) $T = 100\lambda$, $\delta\lambda = 200$ nm; (e) $T = 55\lambda$, $\delta\lambda = 50$ nm; (f) $T = 55\lambda$, $\delta\lambda = 100$ nm (after [39]).

the scattering amplitude. Later, similar experiments were carried out for other types of crystals and neutron beams. The Pendellösung effect has also been predicted and observed in the second-order Bragg scattering of matter waves from a light standing wave acting as a thick grating [35]. Further experiments showed that a quasi-Pendellösung effect can be observed in the Raman–Nath regime [36]. Recently, Savo *et al* have shown experimental evidence that the diffracted wave at the exit of a photonic crystal slab is periodically modulated, as a consequence of the Pendellösung phenomenon (in the infrared region) [37]. Sample thickness dependence of the phenomenon was also shown [38].

In 1996 we predicted that the Pendellösung effect should be observed for certain types of volume holographic gratings, namely when considering a Gaussian and a plane wave interaction [39]. The theoretical transverse intensity distributions behavior showed how the oscillations increased with the sample thickness (>50λ) and the refractive index modulation (>0.01). Figure 8 shows the numerical estimates of the calculated transverse intensity profiles for a Gaussian beam diffracted by volume holographic gratings, for different off-Bragg wavelength detuning and sample thicknesses (see figure caption for detailed parameters).

The theoretical results predicted the oscillatory behavior of the transverse diffracted intensity profile, when the dielectric permittivity modulation of the photomaterial $\Delta\varepsilon$ is large. The actual considered value of $\Delta\varepsilon \sim 0.025$ corresponds to a comparatively large refractive index modulation of $\Delta n \sim 8 \times 10^{-3}$ for $n \sim 1.5$.

Let us now describe briefly the fundamentals of the diffraction of light by volume holographic gratings, based upon the Bragg diffraction regime and Kogelnik's coupled wave theory [12]. The modulated dielectric permittivity of the holographic grating material can be expressed as

$$\varepsilon_r = \varepsilon_{r0} + \varepsilon_n + \varepsilon_{r1} \cos\left(\vec{K} \cdot \vec{r}\right) \tag{5}$$

where ε_{r1} is the dielectric permittivity modulation, ε_{r0} is the dielectric permittivity of the material before exposure and ε_n is the dielectric permittivity change caused by the exposure and holographic development. $\vec{K}$ is the grating vector and $\vec{r}$ is the position vector, here considered as a two-dimensional one of $(x, y, 0)$. According to Kogelnik's coupled wave theory and considering the one-dimensional case under paraxial approximation, the amplitude reflected by a slanted transmission grating is

$$R(x) = \cos\left(\frac{\kappa x}{\sqrt{\cos\theta_1 \cos\theta_2}}\right) \tag{6}$$

where $\kappa = \beta\varepsilon_{r1}/4\varepsilon_{r0}$ is the coupling coefficient, β is the modulus of the wavevector, and θ_1 and θ_2 are the propagation angles of the respective waves. The transmitted amplitude is

$$S(x) = -\mathrm{i}\sqrt{\frac{\cos\theta_1}{\cos\theta_2}} \sin\left[\frac{\kappa x}{\sqrt{\cos\theta_1 \cos\theta_2}}\right]. \tag{7}$$

The two-wave approximation assumes that the holographic grating operates as a thick hologram, with the Q parameter: $Q = |\vec{K}|^2 T/\beta$ values of $Q > 10$, where T is the thickness of the sample and $|\vec{K}| = 2\pi/\Lambda$ is the modulus of the grating wavevector with period Λ. In the symmetric (unslanted) case, $\theta_1 = \theta_2 = \theta_h$ is the Bragg angle. The energy flux in the grating region is given as the sum of two independent time averaged Poynting vectors associated with transmitted $S(x)$ and diffracted $R(x)$ waves, respectively.

The oscillatory behaviors of $R(x)$ and $S(x)$, as functions of $\kappa x/\cos\theta_h$, describe the coherent transfer of energy back and forth between the transmitted zero-order wave and the Bragg diffracted wave. However, this first-order approximation does not account for the Pendellösung effect. This is because, in a higher-order description of the coupling process, there is a contribution representing a coupling term of the two branches of energy. The dynamical diffraction theory predicts that this third coupling term has an oscillatory behavior for nonabsorbing gratings, with an oscillation period determined by $\gamma = \pi\varepsilon_{r_1} T/2\lambda\varepsilon_{r_0} \cos\theta_h$. According to the dynamic theory of diffraction, this can be described in terms of the Poynting vector for the total field (for a particular polarization state):

$$\vec{S}_\mathrm{T} = \sqrt{\frac{\mu_0}{\varepsilon_0}}\left\langle \vec{S}(\vec{r}, t)\right\rangle = \vec{S}_\mathrm{i} + \vec{S}_\mathrm{d} + \vec{S}_\mathrm{id}. \tag{8}$$

In equation (8) μ_0 and ε_0 are the magnetic susceptibility and dielectric permittivity in vacuum, respectively. The bracket $\langle\,\rangle$ accounts for time average. $\vec{S}_\mathrm{i}$ is the energy flux associated with the wave field corresponding to the incident beam, $\vec{S}_\mathrm{d}$ is the diffracted wave field energy flux and $\vec{S}_\mathrm{id}$ is the coupling term between the two. For the Pendellösung effect $\vec{S}_\mathrm{id} \propto$

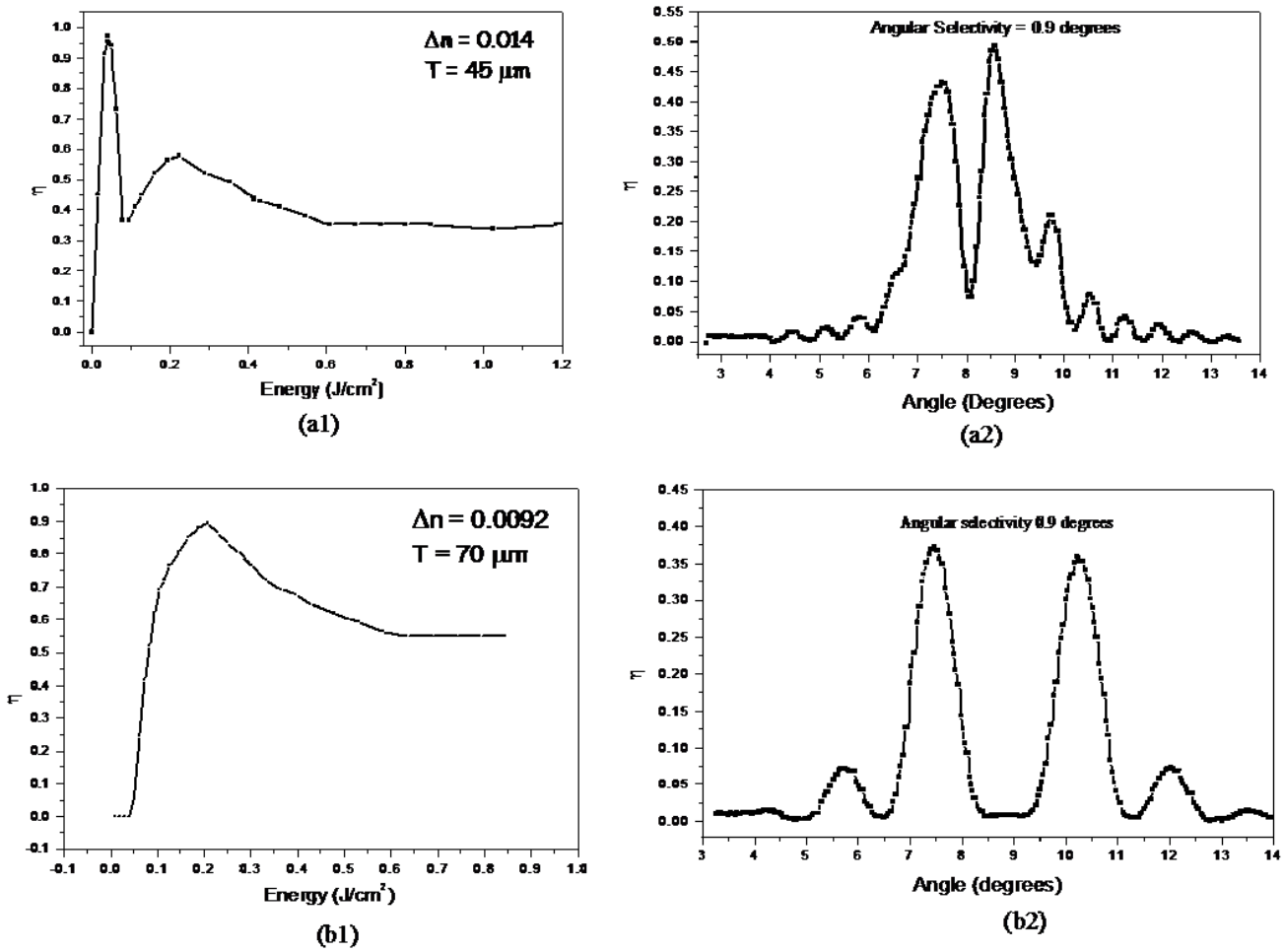

Figure 9. Experimental evidence of diffracted light overmodulation in thick holographic gratings recorded in a photopolymerizable glass with large Δn. (a1) and (b1): diffraction efficiency evolution with exposure. (a2) and (b2): oscillation of the angular selectivity with the angle of incidence. T: sample thickness, Δn: refractive index modulation. Both (a) and (b) were obtained for readout beam incident at the center of the grating.

$\cos(\gamma)$. The coupling term shifts the energy flow around the average direction associated with directions of orders $m = 0$ and $m = -1$, respectively, in a periodic fashion proportionally to γ and showing a sinusoidal variation with the depth of the grating.

3.3.2. Experimental observation of Pendellösung effect. In hybrid organic–inorganic material incorporating HRIS, volume holographic gratings were recorded with high diffraction efficiency and large Δn, allowing for the first experimental observation of the Pendellösung effect in the optical band [40]. Figure 9 shows the experimental results obtained in our photopolymerizable sol–gel glass incorporating the Zr-based HRIM, for two different sample thicknesses, namely 45 and 70 μm. The recorded transmission unslanted grating has a spatial period of 500 lines mm^{-1}. The Klein–Cook parameter is $Q = 62$, hence the Bragg regime holds. The grating was probed using an He–Ne laser, with a spot size of approximately 10% of the grating size. The sample was illuminated in the center position of the grating. We observe the anomalous modulation of the angular selectivity, while maintaining the same diffraction efficiency value of the angular selectivity for each single maximum.

The sequence of images recorded with a CCD camera at the position of the first diffracted order are displayed in figure 10. Each image corresponds to the readout beam at the angle denoted in the figure, for an angular range -10 to $+10$ and for the grating width of 5.3 mm. A change in the angle of the incident beam in the presence of overmodulation results in the energy transfer and hence in a change in the intensity distribution in the diffracted light pattern, yielding the optical Pendellösung fringes. The peaks of maximum energy correspond to $-2°$ and $+2°$, respectively.

The Zr-based HRIM allows for tailoring the material holographic properties to achieve the overmodulation regime while maintaining high diffraction efficiency. This observation of the Pendellösung effect demonstrates that the energy flux transfer, previously observed with electrons and slow neutron beams, exists also in the optical band (visible). This result suggests that modal control based upon the refractive index modulation gradient is feasible in the classical framework of light diffraction. The Pendellösung effect is an interesting

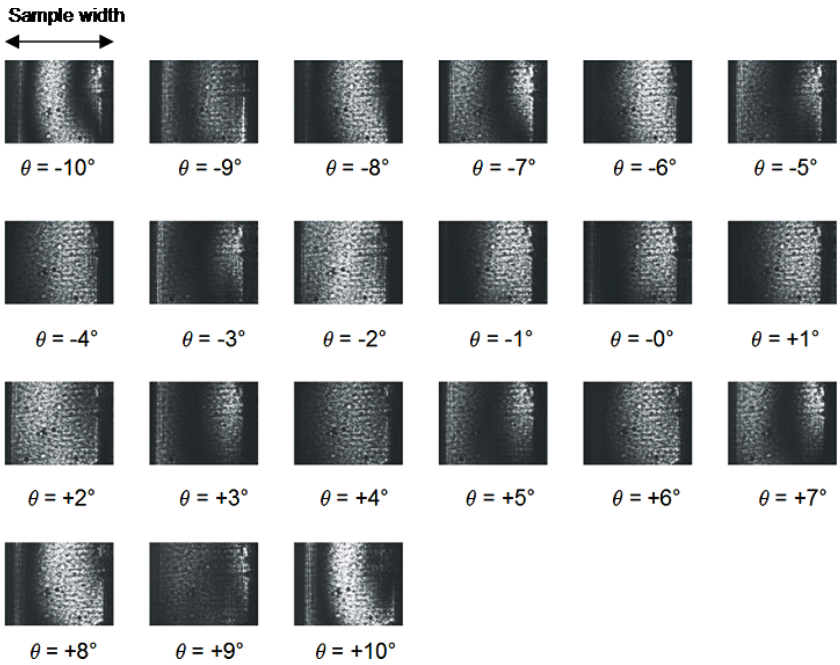

Figure 10. Experimental observation of optical Pendellösung fringes. A sequence of images recorded with a CCD camera for different incident beam angles. The images correspond to the first diffracted order spatial distribution. The peaks of maximum energy correspond to $-2°$ and $+2°$, respectively. The grating width is 5.3 mm. After [40].

phenomenon that can potentially be used in various fields, including the investigation of the structural properties of volume holographic gratings and the development of novel holographic optical elements and devices.

4. Conclusions

We reviewed advances in the development of photopolymerizable sol–gel nanocomposites for holographic recording. We discussed several relevant aspects concerning these materials, including high refractive index and diffraction efficiency, refractive index enhancement using high refractive index molecular species, optical scattering reduction compared to nanoparticle-based materials, fundamental mechanisms of grating formation and co-directional diffusion, and the first experimental observation of the Pendellösung effect in the optical band. Today, several advanced sol–gel holographic materials have become available with interesting niche applications in a variety of fields in research and industry. These nanocomposite materials are particularly promising since they can benefit from synergies arising from a combination of different physical and chemical properties and specific optical functionalities in a single matrix.

Acknowledgments

We thank Oscar Martínez-Matos, Francisco del Monte and José A Rodrigo for invaluable help and many insightful discussions. The financial support of the Spanish Ministry of Education and Science (project no. TEC2005-02180) is acknowledged.

References

[1] Arago F 1839 *C. R. Acad. Sci., Paris* **9** 255
[2] Crawford H E 1960 *Proc. Technical Association of the Graphic Arts* p 193 TAGA Abstracts
[3] Close D H, Jacobson A D, Margerum J D, Brault R J and Mcclung F J 1969 *Appl. Phys. Lett.* **14** 159
[4] Lessard R A and Thompson B J (ed) 1995 *Selected Papers on Photopolymers* (*SPIE Milestone Series* vol 114) (Bellingham, WA: SPIE)
[5] Calvo M L and Cheben P 2008 Fundamentals and advances in holographic materials for optical data storage *Advances in Information Optics and Photonics* vol 6, ed A T Friberg and R Dändliker (Bellingham: SPIE Press) chapter 15 (International Commission for Optics)
[6] Ebelmen J J 1844 *C. R. Acad. Sci.* **19** 398
[7] Schnoes M G, Dhar L, Schilling M L, Patel S S and Wiltzius P 1999 *Opt. Lett.* **24** 658
[8] Ramos G, Alvarez-Herrero A, Belenguer T, Del Monte F and Levy D 2004 *Appl. Opt.* **43** 4018
[9] Cheben P, Belenguer T, Núñez A, Del Monte F and Levy D 1996 *Opt. Lett.* **21** 1857
[10] Cheben P and Calvo M L 2001 *Appl. Phys. Lett.* **78** 1490
[11] Cheben P and Calvo M L 2007 *US Patent Specification* 7163769 Photosensitive material and process of making same
[12] Kogelnik H 1969 *Bell Syst. Tech. J.* **48** 2909
[13] Cheben P, Del Monte F, Worsfold D J, Carlsson D J, Grover C P and Mackenzie J D 2000 *Nature* **408** 64
[14] Suzuki N and Tomita Y 2004 *Appl. Opt.* **43** 2125
[15] Suzuki N, Tomita Y and Kojima T 2002 *Appl. Phys. Lett.* **81** 4121
[16] Sanchez C, Escuti M J, van Heesch C, Bastiaansen C W M, Broer D J, Loos J and Nussbaumer R 2005 *Adv. Funct. Mater.* **15** 1623
[17] Calvo M L, Cheben P, Martinez-Matos O, Rodrigo J A and Del Monte F 2007 *Proc. SPIE* **6785** V7850
[18] Del Monte F, Martínez-Matos O, Rodrigo J A, Calvo M L and Cheben P 2006 *Adv. Mater.* **18** 2014

[19] Coburn W S and Haines K A 1971 *Appl. Opt.* **10** 1636
[20] Suzuki N, Tomita Y, Ohmori K, Hidaka M and Chikama K 2006 *Opt. Express.* **14** 12712
[21] Frantz J A, Kostuk R K and Waldman D A 2001 *Proc. SPIE* **4296** 267
[22] De Miguel-Sanz E M, Carrascosa M and Arizmendi L 2002 *Phys. Rev.* B **65** 165101
[23] Kneipp C, Gallego S, Ortuño M, Márquez A, Alvarez M L, Beléndez A and Pascual I 2003 *J. Opt. Soc. Am.* B **20** 2052
[24] Gallego S, Marquez A, Mendez D, Neipp C, Ortuno M, Belendez E, Fernandez E and Pascual I 2008 *Appl. Phys. Lett.* **92** 073306
[25] Blaya S, Murciano A, Acebal P, Carretero L, Ulibarrena M and Fimia A 2004 *Appl. Phys. Lett.* **84** 4765
[26] Gallego-Gomez F, Del Monte F and Meerholz K 2008 *Nat. Mater.* **7** 490
[27] Martinez-Matos O, Calvo M L, Rodrigo J A, Cheben P and Del Monte F 2007 *Appl. Phys. Lett.* **91** 141115
[28] Klein W R and Cook B D 1967 *IEEE Trans. Son. Ultrason.* **14** 123
[29] Piazolla S and Jenkins B K 2000 *J. Opt. Soc. Am.* B **17** 1147
[30] Tomita Y, Furushima K, Ochi K, Ishizu K, Tanaka A, Ozawa M, Hidaka M and Chikama K 2006 *Appl. Phys. Lett.* **88** 071103–1
[31] Däschner W, Larsson M and Lee S H 1995 *Proc. 45th Electronic Components and Technology Conf.* pp 1283–5, Cat. No.95CH3582-0
[32] Ewald P P 1916 *Ann. Phys., Lpz.* **49** 1
[33] Batterman B W and Cole H 1964 *Rev. Mod. Phys.* **36** 681
[34] Shull C G 1968 *Phys. Rev. Lett.* **21** 1585
[35] Dürr S, Kunze S and Rempe G 1996 *Quantum Semiclass. Opt.* **8** 531
[36] Keller C, Schmiedmayer J, Zeilinger A, Nonn T, Dürr S and Rempe G 1999 *Appl. Phys.* B **69** 303
[37] Savo S, Di Gennaro E, Miletto C, Andreone A, Dardano P, Moretti L and Mocella V 2008 *Opt. Express* **16** 9097
[38] Mocella V 2005 *Opt. Express* **13** 1361
[39] Cheben P and Calvo M L 1996 *J. Opt. Soc. Am.* A **13** 131
[40] Calvo M L, Cheben P, Martinez-Matos O, del Monte F and Rodrigo J A 2006 *Phys. Rev. Lett.* **97** 084801